Optically monitoring voltage in neurons by photo-induced electron transfer through molecular wires

Evan W. Miller[a], John Y. Lin[a], E. Paxon Frady[b], Paul A. Steinbach[a,c], William B. Kristan, Jr.[d], and Roger Y. Tsien[a,c,e,1]

[a]Department of Pharmacology, [b]Neurosciences Graduate Group, [d]Division of Biological Sciences, [e]Department of Chemistry and Biochemistry, and [c]Howard Hughes Medical Institute, University of California at San Diego, La Jolla, CA 92093

Contributed by Roger Y. Tsien, December 21, 2011 (sent for review November 26, 2011)

Fluorescence imaging is an attractive method for monitoring neuronal activity. A key challenge for optically monitoring voltage is development of sensors that can give large and fast responses to changes in transmembrane potential. We now present fluorescent sensors that detect voltage changes in neurons by modulation of photo-induced electron transfer (PeT) from an electron donor through a synthetic molecular wire to a fluorophore. These dyes give bigger responses to voltage than electrochromic dyes, yet have much faster kinetics and much less added capacitance than existing sensors based on hydrophobic anions or voltage-sensitive ion channels. These features enable single-trial detection of synaptic and action potentials in cultured hippocampal neurons and intact leech ganglia. Voltage-dependent PeT should be amenable to much further optimization, but the existing probes are already valuable indicators of neuronal activity.

Fluorescence imaging can map the electrical activity and communication of multiple spatially resolved neurons and thus complements traditional electrophysiological measurements (1, 2). Ca^{2+} imaging is the most popular of such techniques, because the indicators are well-developed (3–6), highly sensitive (5, 6), and genetically encodable (7–13), enabling investigation of the spatial distribution of Ca^{2+} dynamics in structures as small as dendritic spines and as large as functional circuits. However, because neurons translate depolarizations into Ca^{2+} signals via a complex series of pumps, channels, and buffers, fluorescence imaging of Ca^{2+} transients cannot provide a complete picture of electrical activity in neurons. Observed Ca^{2+} spikes are temporally low-pass filtered from the initial depolarization and provide limited information regarding hyperpolarizations and subthreshold events. Direct measurement of transmembrane potential with fluorescent indicators would provide a more accurate account of the timing and location of neuronal activity. Despite the promise of fluorescent voltage-sensitive dyes (VSDs), previous classes of VSDs have each been hampered by some combination of insensitivity, slow kinetics (14–16), heavy capacitative loading (17–21), lack of genetic targetability, or phototoxicity. Two of the more widely used classes of VSDs, electrochromic and FRET dyes, illustrate the problems associated with developing fast and sensitive fluorescent VSDs.

Electrochromic dyes respond to voltage through a direct interaction between the chromophore and the electric field (Scheme 1*A*). This Stark effect leads to small wavelength shifts in the absorption and emission spectrum. Because the electric field directly modulates the energy levels of the chromophore, the kinetics of voltage sensing occur on a timescale commensurate with absorption and emission, resulting in ultrafast (fs to ps) hypso- or bathochromic shifts many orders-of-magnitude faster than required to resolve fast spiking events and action potentials in neurons. This small wavelength shift dictates that the fluorescence signal can be best recorded at the edges of the spectrum, where intensity varies most steeply as a function of wavelength. The largest linear responses are −28% ΔF/F per 100 mV (22), although more typical values are ∼10% per 100 mV (23, 24). Photo-induced electron transfer (PeT)-based Ca^{2+} probes, such as fluo-3, give ΔF/F values of up to 150% for action potentials in cultured hippocampal neurons (25). Therefore, although electrochromic dyes can keep pace with fast voltage oscillations in neurons, their insensitivity limits the systems in which these dyes can successfully report on voltage changes.

FRET-based voltage sensors use lipophilic anions that intercalate into the cellular membrane and distribute between the inner and outer leaflets depending upon the transmembrane potential (Scheme 1*B*). The Nernstian distribution is monitored by a second fluorophore immobilized on one side of the membrane, which undergoes FRET preferentially with the mobile anions on the same side of the membrane. Translocation of the lipophilic anion through the lipid bilayer governs the kinetics of voltage sensing, which can be in the millisecond range. Although these two-component systems can give large changes in intensity (5–34%) (21) or ratio (80% per 100 mV) (15), the slow translocation of mobile charges in the plasma membrane introduces a capacitative load and hampers the ability of the reporter to monitor fast changes.

To combine the best features of electrochromic and FRET-based VSDs, we have now tested a unique mechanism for voltage sensing, PeT through molecular wires. In these PeT sensors, a fluorescent reporter connects to an electron-rich quencher via a molecular wire, which minimizes the exponential distance dependence of intramolecular electron transfer (26) and allows efficient electron transfer over a major fraction of the thickness of the plasma membrane. At resting or hyperpolarized potentials, the transmembrane electric field promotes electron transfer from the quencher to the excited-state fluorophore through the molecular wire, quenching fluorescence (Scheme 1*C*). Depolarization reverses the electric field, hinders electron transfer, and brightens fluorescence (27), just as Ca^{2+} binding dequenches indicators like fluo-3 (28). Electron transfer occurs within pico- to nanoseconds after photon absorption and returns to its initial state within a microsecond (26, 29), slower than the electrochromic mechanism but essentially instantaneous on a biological timescale. Because electron transfer reverses quickly and is driven by photon absorption rather than membrane potential changes, capacitative loading should be negligible, as calculated in the *SI Appendix*. A full electronic charge traverses a Marcus-type thermal activation barrier to sense a large fraction of the membrane voltage, making voltage sensitivity high (30). Quenching of the fluorescent reporter by the electron-rich donor modulates the fluorescence quantum yield independent of wavelength, permitting efficient use of photons for excitation and emission, allowing lower light levels or dye concentrations to be used. We report here the design, synthesis, and application of the VoltageFluor (VF) family of fluorescent sensors as molecular wire PeT-based probes for voltage imaging in neurons.

Author contributions: E.W.M., W.B.K., and R.Y.T. designed research; E.W.M., J.Y.L., E.P.F., and P.A.S. performed research; E.W.M., E.P.F., W.B.K., and R.Y.T. analyzed data; and E.W.M. and R.Y.T. wrote the paper.

The authors declare no conflict of interest.

Freely available online through the PNAS open access option.

[1]To whom correspondence should be addressed. E-mail: rtsien@ucsd.edu.

This article contains supporting information online at www.pnas.org/lookup/suppl/doi:10.1073/pnas.1120694109/-/DCSupplemental.

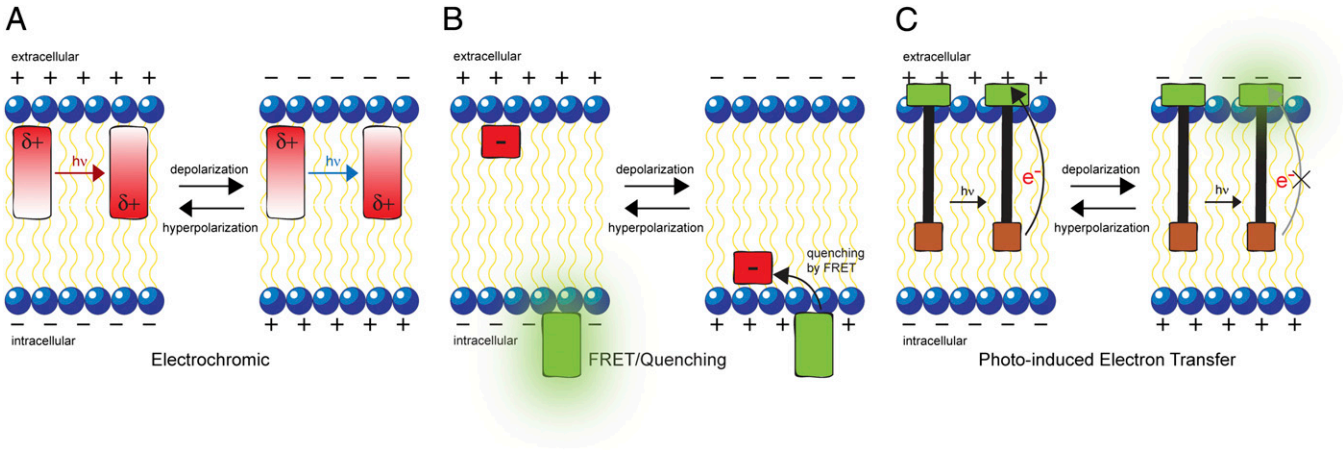

Scheme 1. Mechanisms of fluorescent voltage sensing. (*A*) Electrochromic VSDs sense voltage through the Stark effect, whereby the chromophore interacts directly with the electric field. Absorption of a photon significantly alters the excited state molecular dipole, which at hyperpolarizing potentials is stabilized (*Left*). At depolarizing potentials the charge shift inverted state is destabilized (*Right*). Changes in the energy levels of the chromophore result in small spectral shifts in the emission of the dye. (*B*) FRET-pair voltage sensors use lipophilic anions (red), which partition in a voltage-dependent fashion on the inner or outer leaflet of the membrane. Depolarization causes translocation of the anion, which can now quench the fluorescence of an immobilized fluorophore (green). (*C*) Molecular wire PeT VSDs depend upon the voltage-sensitive electron transfer from an electron-rich donor (orange) through a membrane-spanning molecular wire (black) to a fluorescent reporter (green). At hyperpolarizing potentials, the electric field is aligned antiparallel to the direction of electron transfer, resulting in efficient PeT and quenched fluorescence (*Left*). Depolarization aligns the electric field in the direction of PeT, decreasing the rate of electron transfer and increasing fluorescence (*Right*).

Results

Design and Synthesis of VF Sensors. Our initial voltage sensors incorporate dichlorosulfofluorescein as a membrane-impermeant fluorophore, a *p*-phenylenevinylene (PPV) molecular wire, and *N*, *N*-dimethyl- or dibutylaniline as an electron-rich quencher (Scheme 2). VF1.4.Cl comprises 2,7-dichlorosulfofluorescein connected via one vinylene unit to dibutylaniline (hence VF1.4.Cl). VF2.4.Cl adds a second PPV unit, and VF2.1.Cl features the same configuration, with methyl substituted in place of butyl groups.

Correct positioning of the fluorophore-wire donor within the membrane is vital to take advantage of the vectoral nature of the transmembrane electric field and electron transfer. First, the longitudinal axis of the molecular wire must be normal to the plane of the plasma membrane, to sample the full electric field. Second, dye molecules must all align in the same direction to avoid canceling out the electron transfer effect. Positioning the fluorophore at the extracellular leaflet of the membrane ensures fluorescence brightening upon depolarization; the opposite orientation of PeT would give fluorescence quenching upon depolarization.

The negatively charged sulfofluorescein will preclude dye internalization and force an orientation in which the fluorophore adsorbs to the outer leaflet of the plasma membrane, with the lipophilic molecular wire and alkyl aniline dangling into the lipid bilayer. As an intervening spacer, PPV molecular wires are an ideal choice because of their low attenuation values (26), synthetic tractability, and demonstrated ability to conduct current through lipid bilayers (31). Anilines are common PeT donors and the dialkyl groups should enhance uptake into the plasma membrane.

A modular synthetic design both allows for rapid generation of the voltage sensors and enables future derivatization (Scheme 2 and *SI Appendix*). Coupling of the molecular wire styrene unit **1**, available in one step from 4-di-butylaminobenzaldehyde, with iodo-functionalized dichlorosulfofluorescein **2** via a Pd-catalyzed Heck reaction gives VF1.4.Cl in good yield. An analogous reaction with molecular wire **3**, available in two steps from **1**, gives VF2.4.Cl in 70% yield. A parallel reaction beginning from styrene **4** furnishes VF2.1.Cl in good yield. All dyes feature emission and excitation profiles typical of dichlorofluoresceins (VF1.4.Cl: λ_{max} = 521 nm, ε = 93,000 $M^{-1}{\cdot}cm^{-1}$, λ_{em} = 534 nm, Φ = 0.24; VF2.4.Cl:

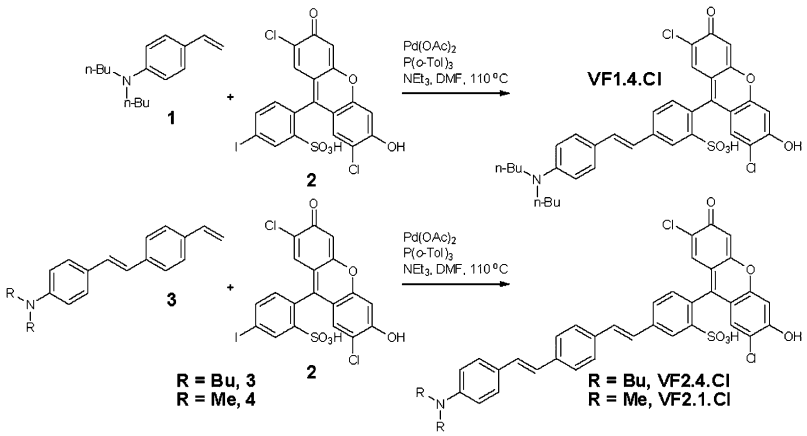

Scheme 2. Synthesis of VF probes.

λ_{max} = 522 nm, ε = 97,000 $M^{-1}{\cdot}cm^{-1}$, λ_{em} = 536 nm, Φ = 0.054; VF2.1.Cl: λ_{max} = 522 nm, ε = 98 000 $M^{-1}{\cdot}cm^{-1}$, λ_{em} = 535 nm, Φ = 0.057, 5 mM sodium phosphate, pH 9, 0.1% Triton X-100) (*SI Appendix*, Fig. S1). The dibutyl (VFx.4.Cl) dyes stain the cell membranes of HEK293 cells when loaded at a concentration of 2 μM for 15 min at 37 °C in buffer with 0.1% DMSO as cosolvent (Fig. 1*A*, and *SI Appendix*, Fig. S2). VF2.1.Cl requires even lower dye concentrations (100 nM) and gives bright staining of HEK cell membranes, which is likely to be because of the greater aqueous solubility of VF2.1.Cl compared with VF2.4.Cl in aqueous solution (*SI Appendix*, Fig. S2). The membrane retention of the second generation dyes (VF2.x.Cl) is in contrast to di-4-ANEPPS, which at the same loading conditions, shows significant uptake into internal membranes. The bleach rates of the probes were tested in HEK cells and compared with di-4-ANEPPS. The bleach rates for VF1.4.Cl, VF2.4.Cl, and VF2.1.Cl at 7 W/cm^2 were measured to be 3.9 ± 0.1 × 10^{-2} s^{-1}, 1.8 ± 0.1 × 10^{-2} s^{-1}, and 8.0 ± 0.1 × 10^{-3} s^{-1}, respectively. These results are two-, four-, and ninefold smaller than di-4-ANEPPS, which has a bleach rate, under identical illumination conditions, of 6.9 ± 0.1 × 10^{-2} s^{-1}.

Characterization of the Voltage Response of VF Sensors. We characterized the voltage sensitivity of all three indicators by making tight-seal whole-cell recordings of HEK293 cells stained with the VF sensors. Cells were voltage-clamped at −60 mV holding potential and sequentially stepped to depolarizing and hyperpolarizing potentials at 20-mV increments (Fig. 1*B*). For all three dyes, depolarizing steps produced fluorescence increases, whereas hyperpolarizing steps produced fluorescence decreases, in keeping with the proposed PeT mechanism. The fluorescence response is linear over the range of −100 mV to +100 mV (Fig. 1*C*), with voltage sensitivities ΔF/F per 100 mV of 20 ± 1% for VF1.4.Cl and 25 ± 1% for VF2.4.Cl. This statistically significant increase in voltage sensitivity ($P < 0.05$, two-tailed Student *t* test) is expected upon increasing the length of the molecular wire, and is 2.5- to 4-times more sensitive than di-4-ANEPPS, which, in our hands, gives sensitivities of between 6% and 10% ΔF/F per 100 mV. VF2.1.Cl shows fluorescence increases upon depolarization similar to VF2.4.Cl, with a voltage sensitivity of 27 ± 1% per 100 mV. This value is not significantly different from the sensitivity of VF2.4.Cl, suggesting that voltage sensitivity is largely determined by the length of the molecular wire and that the small increase in electron donating ability of the butyl relative to the methyl groups makes only a relatively small contribution to the increased voltage sensitivity of VF2.1.Cl. To investigate the speed of response of VF probes, we again made whole-cell recordings of cells stained with VF2.4.Cl, applied 100-mV depolarizing steps from a holding potential of −60 mV, and recorded both the electrophysiological signals and the optical signals. Fitting the electrophysiological and optical recordings gave identical time constants for both beginning and end of the pulse ($\tau_{ON,\ phys}$ = 139 ± 0.2 μs, $\tau_{ON,\ optical}$ = 138 ± 14 μs, $\tau_{OFF,\ phys}$ = 142 ± 0.4 μs, $\tau_{OFF,\ optical}$ = 147 ± 19 μs), showing that VF2.4.Cl and related sensors do not introduce any detectable lag in their fluorescence response to voltage, consistent with a PeT-based mechanism for voltage sensing (Fig. 2 *A* and *B*).

The fluorescence response of VF2.4.Cl to voltage changes is insensitive to the excitation wavelength, as is true for PeT-based probes, such as fluo-3 and Calcium Green-1. We assayed the wavelength dependence of VF2.4.Cl by changing the excitation wavelength in 5-nm steps and determined that the fluorescence response of VF2.4.Cl to a 100-mV depolarization from a holding potential of −60 mV varied only about 15% when testing wavelengths from 445 to 500 nm (Fig. 2*C*). In comparison, di-4-ANEPPS varies by nearly 100% over its excitation spectrum (32), and the PeT-based Ca^{2+} sensor, Calcium Green-1, varies by ∼20% (*SI Appendix*, Fig. S3). These comparisons show that the wavelength independence of the voltage sensitivity is more consistent with PeT than a wavelength-shifting mechanism, such as electrochromism or solvatochromism (a wavelength shift because of alteration in local solvation).

PeT-based molecular wire sensors do not affect neuronal excitability by capacitative loading. We injected hyperpolarizing current into the Retzius cells of leech ganglia preparations and compared the time constants for these voltage steps in ganglia under different dye loading conditions. The ganglia were stained with dye at three times the working concentration [either VF2.1.Cl or diSBA-C_4-(3) (14)] and compared with unloaded cells. The presence of the translocating dye oxonol 413 substantially increases the capacitative load on the membrane, as measured by the increase in the RC time constant for the hyperpolarizing injection (Fig. 2*D*). On the other hand, ganglia loaded with VF2.1.Cl show no difference from control cells, demonstrating that molecular wire sensors place negligible capacitative load on the cell (Fig. 2*D*), confirming the predictions of the *SI Appendix*.

Detection of Action Potentials by VF2.4.Cl in Mammalian Neurons. To assess whether VF probes can detect action potentials in single trials, we used cultured rat hippocampal neurons. Bath application of 2 μM VF2.4.Cl showed bright cell staining limited to the cell membranes of neurons and their support cells (Fig. 3*A*). We then injected current into a neuron under whole-cell patch-clamp mode to trigger single action potentials and used a high-speed, back-illuminated EMCCD camera to track fast optical signals from VF2.4.Cl, enabling us to resolve action potentials in neurons in single sweeps (Fig. 3*B*). The optical trace matched the physiology trace and gave about a 20% ΔF/F increase in fluorescence and a 16:1 signal-to-noise ratio (SNR) in a single trial. The fact that VF2.4.Cl detected action potentials without spike-timed averaging suggests the possibility of measuring spontaneous action potentials in neurons at sites away from the recording pipette.

Monitoring Spontaneous Activity in Leech Ganglia with VF2.1.Cl. A more stringent test of the usefulness of the PeT-based VSD is to determine whether it can accurately measure subthreshold activity in heterogeneous preparations. For this test we used leech ganglia, because their neurons have been well studied using both

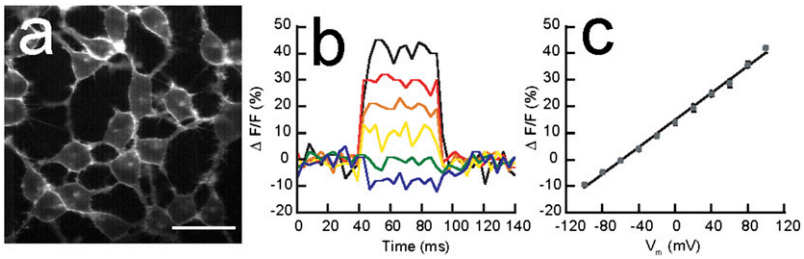

Fig. 1. Characterization of VF sensors in HEK cells. (*A*) Confocal image of HEK 293 cells stained with 2 μM VF2.4.Cl. (Scale bar, 20 μm.) (*B*) Fractional changes in VF2.4.Cl fluorescence during a series of voltage steps to +100 or −100 from a holding potential of −60 mV (40-mV increments). (*C*) Fractional changes in VF2.4.Cl fluorescence from *B* plotted against membrane potential for voltage changes from a holding potential of −60 mV. Each datapoint represents three to four separate measurements. Error bars are SEM.

electrophysiological and other VSD recordings (14, 33–35). We isolated a midbody ganglion and stained it with VF2.1.Cl for 15 min at 22 °C (Fig. 3*C*). Insertion of a sharp electrode (25 MΩ) into a Retzius cell to enabled recording of its spontaneous activity while simultaneously recording the fluorescence signals from the same cell. When sampling at a rate of 50 Hz, the optical recording (Fig. 3*D*, red trace) faithfully followed the subthreshold fluctuations in the electrical recording (black trace). The optically recorded spikes are truncated as a result of undersampling the optical signal; sampling at a higher rate (722 Hz) fully resolved the action potentials, but introduced a significant amount of sampling noise (*SI Appendix*, Fig. S4). Although the action potential was subsampled at just 50 Hz, there is still a reliable transient in the optical trace that indicates the time when an action potential occurs, which is often what is needed.

The PeT-based VSDs show significant improvement in speed and accuracy compared with FRET-based VSDs previously used for leech recordings (33, 36–38), which in turn had superseded electrochromic dyes (14). The improvement in the recording of membrane potential fluctuations is not the result of a greater sensitivity (the ΔF/F for both the FRET and PeT dyes is about 10% per 100 mV in leech recordings), but to a greater SNR. The PeT-based VSD produces a much brighter signal, one that is well above the photon noise levels of the dye and the dark noise level of the camera. Increasing the concentration of the FRET-based dye does increase its SNR, but the consequent increase in the cell's capacitance (Fig. 2*D*) makes the dye useless for recording either action potentials or synaptic potentials. Tests of the toxicity and bleaching of the PeT-based VSD similar to those performed on the FRET-based dyes (14) show that the PeT-based VSD has a slower rate of bleaching and is less toxic than the FRET-based dyes. Hence, considering all measures, the PeT-based VSD performs better than the FRET-based dyes (39).

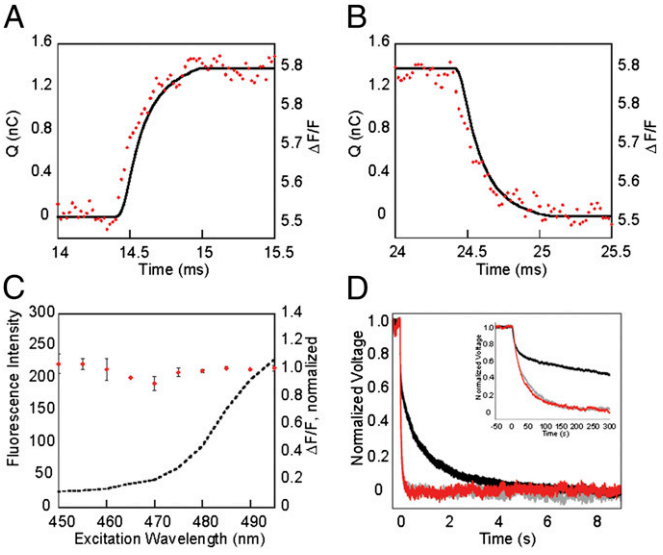

Fig. 2. Characterization of the speed, wavelength sensitivity, and capacitance of the VF2 fluorescence response. (*A*) Rising edge of a 100-mV depolarizing step from −60 mV in HEK cells stained with VF2.4.Cl. (*B*) Falling edge of the same step. Black, solid trace is the integrated current measured electrophysiologically; red points are the optical recording. Time constants are calculated by fitting a monoexponential equation to each side of the step. Traces are the average of 100 sequential trials. (*C*) Voltage sensitivity vs. excitation wavelength. The normalized response of VF2.4.Cl to a 100 mV depolarization from −60 mV in HEK cells is plotted in red, and the excitation spectrum in HEK cells is the dotted black line. Error bars are SEM for $n = 3$ experiments. (*D*) Measurement of capacitative loading in leech Retzius cells. Traces show the normalized voltage decay following hyperpolarizing current injection into Retzius cell stained with 3× VF2.1.Cl (red trace), 3× oxonol 413 (black trace), or nothing (gray trace). (*Inset*) An expanded time scale revealing no difference between cells stained with VF2.1.Cl and control cells.

Discussion

Optimal VSDs would have large, fast responses to changes in voltage, place little or no capacitative load on the membrane, photobleach slowly with minimal photodynamic damage, and would be synthetically tractable for rational chemical modification and genetic targetability. We believe that the VF family of PeT-based probes surpass previous VSD classes by these criteria. The three PPV molecular wire, PeT-based molecules we tested (VF1.4.Cl, VF2.4.Cl, and VF2.1.Cl) exhibit good membrane staining and 20–27% ΔF/F per 100-mV increases in fluorescence upon depolarization in HEK cells. These molecules possess the fast kinetics ($\tau_{ON/OFF}$ <<140 μs) and wavelength-independent voltage sensitivity consistent with a PeT mechanism for sensing voltage. Measurements of capacitance in leech neurons show that an insignificant amount of capacitative load is placed on the membrane. The advantages of PeT-based dyes over both electrochromic and FRET-based methods for optical voltage sensing are described below and summarized in Table 1. A fourth technique, making use of genetically encoded voltage sensors, offers a promising method for optically monitoring voltage changes because the fluorescent proteins can be targeted to cells of interest, thereby increasing the SNR of the fluorescence response. In practice, however, fluorescent protein voltage sensors suffer from low sensitivity [0.5% (40) to 10% Δ F/F per 100 mV (41)], nonlinear responses (42) and slow kinetics (tens to hundreds of milliseconds). Newer efforts have made use of proton translocation within bacterial rhodopsins (43), but although these show large voltage sensitivities, the response time is still in the millisecond range, quantum efficiencies are very low, and their expression limited to prokaryotic systems. Voltage-driven translocation of ions through the membrane will generally add much more capacitative load than electron translocation during transient excited states (44).

VSDs using a PeT-based molecular wire approach should be highly sensitive. Because a full electronic charge travels through a substantial fraction of the transmembrane voltage (11 Å for VF1.4.Cl, 17 Å for VF2.4.Cl and VF2.1.Cl, or 37% and 57% of the 30 Å low-dielectric constant core of the plasma membrane) the change in driving force for PeT is large. For example, a 100-mV depolarization changes the PeT driving force by 0.05 eV (one electron × half of 100-mV potential, or 0.05 V). Because PeT is a thermally controlled process, the value of 0.05 eV is large relative to the value of kT at 300 K (0.026 eV), yielding a large dynamic range between the rates of PeT at resting and depolarized potentials. FRET-based VSDs will have similar sensitivities; lipid-soluble mobile anions transverse distances calculated to be between 0.4 (16) and 0.6 (45) of the total membrane width, resulting in ΔG of ∼0.05 eV for 100-mV depolarization, compared with a kT of 0.026 eV for the thermally activated process.

In contrast, electrochromic dyes have smaller ΔG values, 0.003 (46) to 0.02 (47) eV, and larger comparison energies. Because the interaction is a photochemically controlled process, the energy of the exciting photon is the comparison energy, which is 1.5–2 eV for dyes in the blue-to-green region of the spectrum. Therefore, PeT and FRET dyes have large changes in energy versus their comparison energy (0.05 eV vs. 0.026 eV), giving high sensitivities; electrochromic dyes have small changes compared with the excitation photon (0.003–0.02 eV vs. 2 eV), producing low voltage sensitivity.

The nature of the PeT mechanism also predicts that the kinetics of voltage sensing will be fast; forward electron transfer occurs on the nanosecond timescale as fluorescence is quenched, and back-electron transfer completes the cycle and occurs on a microsecond timescale or faster, meaning that the slow step, electron-hole recombination, finishes a full three orders-of-magnitude faster than an action potential. Electrochromic dyes

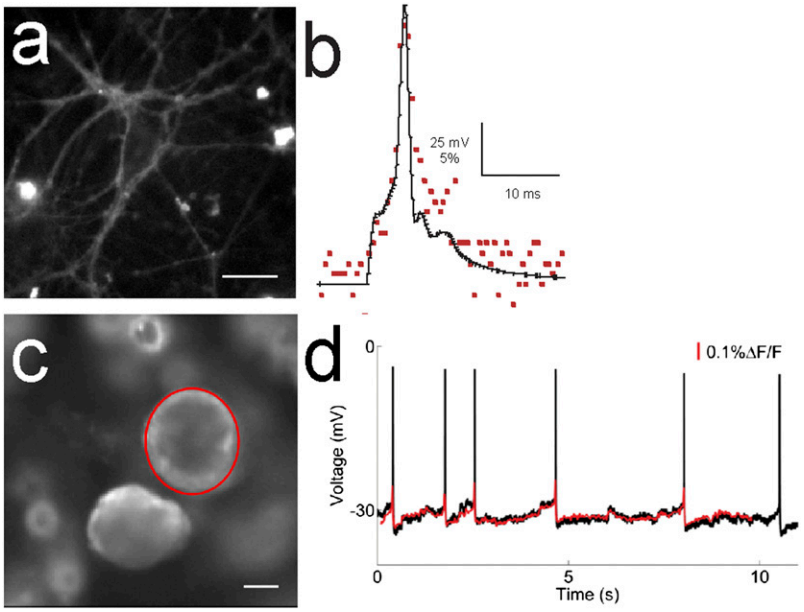

Fig. 3. VF2 dyes resolve action potentials in neurons. (*A*) Rat hippocampal neurons stained with 2 μM VF2.4.Cl for 15 min show strong membrane staining. (Scale bar, 20 μm.) (*B*) VF2.4.Cl can detected evoked action potentials in rat hippocampal neurons in single trials. The black trace is the recorded electrophysiology signal. Individual points represent the optical signal from VF2.4.Cl captured with a high speed EMCCD camera at a rate of 2 kHz. (*C*) Optical imaging of spontaneous activity in leech Retzius cells using the dye VF2.1.Cl. Desheathed midbody leech ganglion stained with 200 nM VF2.1.Cl for 15 min. Pixels within the region of interest (red circle around a single Retzius cell body) were averaged in each frame to produce the optical trace. (Scale bar, 25 μm.) (*D*) Simultaneous optical and electrophysiological recording of spontaneous activity in cell from *C*. The red trace is the hi-pass filtered VF2.1.Cl signal, sampled at 50 Hz. The black trace is the electrophysiological recording, sampled at 10 kHz. The optical trace shows near-perfect matching of the subthreshold membrane potential and a clear detectable signal indicating action potentials. Action potentials have variable amplitudes in the optical traces because of the relatively slow optical sampling rate (*SI Appendix*, Fig. S4).

display even faster kinetics, as forward charge shift occurs with absorbance, on the femtosecond time scale, and resolves itself upon emission of a photon, enabling these dyes to keep time with the fastest spiking neurons. FRET pair VSDs depend upon the migration of a lipophilic anion through an unstirred lipid bilayer and display kinetics in the millisecond-to-second time regime, limiting their application to monitoring only slow transients.

Because PeT shuttles an electron across the membrane and back on a microsecond or faster timescale, driven by photons rather than membrane potential changes, no capacitative loading should be observed. The same holds true for electrochromic dyes, which transfer electrons on even faster time scales. One disadvantage of electrochromic dyes is that they require the entire voltage-sensing chromophores to be rigid to enable π orbital overlap, quantum yield, efficient charge transfer, and maximization of voltage sensitivity (22). Such rigidity hinders synthesis and water solubility and may explain why electrochromic dyes are not improved by lengthening their chromophores. PeT probes do not require the entire molecular wire to be rigidly coplanar, and synthesis of longer wires is feasible.

PeT-sensing allows the entire emission spectrum to be used for monitoring voltage, because the quenching mechanism alters the Φ_{Fl}, decreasing the brightness of the dye, and does not shift the wavelength as do electrochromic methods. Because photons are not wasted, this allows lower intensity light to be used in experiments, reducing phototoxicity and increasing the duration of experimental procedures. The performance of electrochromic dyes has plateaued over four decades of development. Excitation at the far-red edge of the spectrum gives voltage sensitivities ranging from −35% to −52% ΔF/F per 100 mV; however, at the edge of the spectrum, the intensity is far below the peak and the voltage response becomes nonlinear (48).

Several limitations of the VF dyes remain to be addressed. VF derivatives are not yet genetically targetable. The sensors are readily taken up by the cell membranes of all tissue, increasing nonresponsive background fluorescence and decreasing the SNR. For heterogeneous preparations, such as intact leech ganglia and brain slices, this becomes an increasingly important issue, and one method to address this concern is through the genetic targeting of VSDs. VF sensors lend themselves to chemical derivatization, and efforts are underway to modify VF probes for targeting to genetically defined circuits of neurons.

Another drawback is that VF PeT sensors are not as sensitive to voltage as hoped. Our first derivatives show sensitivities ranging from 20–27% ΔF/F per 100 mV, and the most sensitive of existing electrochromic dyes exhibit −28% ΔF/F per 100-mV sensitivities in the linear range (47). Although it is encouraging that the first derivatives display sensitivities on a level approaching the most

Table 1. Summary of VSD attributes

Attribute	Electrochromic	FRET	PeT
Nature of translocating charge	Electron	Lipid soluble anion	Electron
Forward charge shift occurs when	Photon absorption	Membrane depolarization	Quenching
Reverse charge shift occurs when	Photon emission or radiationless decay	Membrane repolarization	Electron-hole recombination
Fractional charge x Fraction of total voltage	~0.1	0.4–0.6	~0.5
Δ energy for 100 mV ΔV	0.003–0.02 eV	0.06 eV	0.05 eV
Comparison energy	Photon energy	kT	kT
	1.5–2 eV	0.026 eV	0.026 eV
Extended rigid fluorophore needed?	Yes	No	No
Use full ex/em band	No	Yes	Yes
Sensitivity Δ F/F per mV	Low	High	High
Speed	fs	ms–s	ns–μs
Capacitative loading	None	Significant	None

sensitive electrochromic dyes, we believe ample chemical space exists for improving the voltage sensitivity of molecular wire platforms. Because the voltage sensitivity is controlled by PeT, the efficiency of PeT can be rationally tuned (49) by altering the electron affinities of the donor, wire, and acceptor to maximize the fluorescence turn-on in response to depolarizations. Additionally, extending the molecular wire to span an even greater distance across the plasma membrane should increase sensitivity as the transferred electron samples more of the electric field. The modular nature of the VF synthesis allows for rapid interchange of coupling partners to quickly assemble and assess the voltage sensitivity of an array of compounds.

In summary, we present a unique method for monitoring voltage in neurons based on the voltage-sensitive PeT from an electron-rich donor to fluorescent reporter attached via a membrane-spanning molecular wire. The VF family of sensors have large, linear, turn-on fluorescence responses to depolarizing steps (20–27% $\Delta F/F$ per 100 mV), fast kinetics ($\tau << 140$ μs), and negligible capacitative loading. VF2.4.Cl can detect and resolve evoked action potentials in primary culture hippocampal neurons, and VF2.1.Cl can monitor spontaneous spiking and synaptic potentials in leech Retzius cells with sensitivity and time-course essentially identical to the recorded electrophysiology signal. VF sensors provide a practical alternative to currently available VSDs, and future derivatives of the molecular wire platform will increase our ability to optically monitor the temporal and spatial dynamics of neuronal activity in defined circuits of neurons.

Methods

Imaging, electrophysiology, cell culture, leech imaging and electrophysiology, and data analysis methods are available in *SI Appendix*. Theoretical considerations of capacitative load are included in *SI Appendix*. Dyes were synthesized using standard synthetic procedures detailed in *SI Appendix*.

ACKNOWLEDGMENTS. We thank David Kleinfeld for use of a photomultiplier photometer and Intelligent Imaging Innovations and Photometrics for use of the Evolve 128 camera. This work was supported in part by the Howard Hughes Medical Institute and US National Institute of Neurological Disorders and Stroke Grant R37 NS027177 (to R.Y.T.); National Institutes of Health Grant MH43396 and National Science Foundation Grant IOB-0523959 (to W. B.K.); the National Institute of Biomedical Imaging and Bioengineering for Postdoctoral Fellowship F32 EB012423 (to E.W.M.); and National Institutes of Health Training Grants EB009380 and MH020002 (to E.P.F.).

1. Scanziani M, Häusser M (2009) Electrophysiology in the age of light. *Nature* 461: 930–939.
2. Peterka DS, Takahashi H, Yuste R (2011) Imaging voltage in neurons. *Neuron* 69:9–21.
3. Poenie M, Alderton J, Tsien RY, Steinhardt RA (1985) Changes of free calcium levels with stages of the cell division cycle. *Nature* 315:147–149.
4. Tsien RY, Rink TJ, Poenie M (1985) Measurement of cytosolic free Ca2+ in individual small cells using fluorescence microscopy with dual excitation wavelengths. *Cell Calcium* 6:145–157.
5. Grynkiewicz G, Poenie M, Tsien RY (1985) A new generation of Ca2+ indicators with greatly improved fluorescence properties. *J Biol Chem* 260:3440–3450.
6. Minta A, Kao JP, Tsien RY (1989) Fluorescent indicators for cytosolic calcium based on rhodamine and fluorescein chromophores. *J Biol Chem* 264:8171–8178.
7. Nagai T, Sawano A, Park ES, Miyawaki A (2001) Circularly permuted green fluorescent proteins engineered to sense Ca2+. *Proc Natl Acad Sci USA* 98:3197–3202.
8. Miyawaki A, et al. (1997) Fluorescent indicators for Ca2+ based on green fluorescent proteins and calmodulin. *Nature* 388:882–887.
9. Tian L, et al. (2009) Imaging neural activity in worms, flies and mice with improved GCaMP calcium indicators. *Nat Methods* 6:875–881.
10. Mank M, et al. (2008) A genetically encoded calcium indicator for chronic in vivo two-photon imaging. *Nat Methods* 5:805–811.
11. Heim N, Griesbeck O (2004) Genetically encoded indicators of cellular calcium dynamics based on troponin C and green fluorescent protein. *J Biol Chem* 279: 14280–14286.
12. Palmer AE, et al. (2006) Ca2+ indicators based on computationally redesigned calmodulin-peptide pairs. *Chem Biol* 13:521–530.
13. Horikawa K, et al. (2010) Spontaneous network activity visualized by ultrasensitive Ca (2+) indicators, yellow Cameleon-Nano. *Nat Methods* 7:729–732.
14. Cacciatore TW, et al. (1999) Identification of neural circuits by imaging coherent electrical activity with FRET-based dyes. *Neuron* 23:449–459.
15. González JE, Tsien RY (1997) Improved indicators of cell membrane potential that use fluorescence resonance energy transfer. *Chem Biol* 4:269–277.
16. González JE, Tsien RY (1995) Voltage sensing by fluorescence resonance energy transfer in single cells. *Biophys J* 69:1272–1280.
17. Sjulson L, Miesenböck G (2008) Rational optimization and imaging in vivo of a genetically encoded optical voltage reporter. *J Neurosci* 28:5582–5593.
18. Akemann W, Lundby A, Mutoh H, Knöpfel T (2009) Effect of voltage sensitive fluorescent proteins on neuronal excitability. *Biophys J* 96:3959–3976.
19. Wang D, Zhang Z, Chanda B, Jackson MB (2010) Improved probes for hybrid voltage sensor imaging. *Biophys J* 99:2355–2365.
20. Bradley J, Luo R, Otis TS, DiGregorio DA (2009) Submillisecond optical reporting of membrane potential in situ using a neuronal tracer dye. *J Neurosci* 29:9197–9209.
21. Chanda B, et al. (2005) A hybrid approach to measuring electrical activity in genetically specified neurons. *Nat Neurosci* 8:1619–1626.
22. Hubener G, Lambacher A, Fromherz P (2003) Anellated hemicyanine dyes with large symmetrical solvatochromism of absorption and fluorescence. *J Phys Chem B* 107: 7896–7902.
23. Grinvald A (1983) Fluorescence monitoring of electrical responses from small neurons and their processes. *Biophys J* 42:195–198.
24. Fluhler E, Burnham VG, Loew LM (1985) Spectra, membrane binding, and potentiometric responses of new charge shift probes. *Biochemistry* 24:5749–5755.
25. Jacobs JM, Meyer T (1997) Control of action potential-induced Ca2+ signaling in the soma of hippocampal neurons by Ca2+ release from intracellular stores. *J Neurosci* 17: 4129–4135.
26. Davis WB, Svec WA, Ratner MA, Wasielewski MR (1998) Molecular-wire behaviour in p-phenylenevinylene oligomers. *Nature* 396:60–63.
27. de Silva AP, et al. (1995) New fluorescent model compounds for the study of photoinduced electron transfer: The influence of a molecular electric field in the excited state. *Angew Chem Int Ed Engl* 34:1728–1731.
28. Adams SR (2010) How calcium indicators work. *Cold Spring Harbor Protocols* 2010: pdb.top70.
29. de la Torre G, Giacalone F, Segura JL, Martín N, Guldi DM (2005) Electronic communication through pi-conjugated wires in covalently linked porphyrin/C60 ensembles. *Chemistry* 11:1267–1280.
30. Li LS (2007) Fluorescence probes for membrane potentials based on mesoscopic electron transfer. *Nano Lett* 7:2981–2986.
31. Garner LE, et al. (2010) Modification of the optoelectronic properties of membranes via insertion of amphiphilic phenylenevinylene oligoelectrolytes. *J Am Chem Soc* 132: 10042–10052.
32. Montana V, Farkas DL, Loew LM (1989) Dual-wavelength ratiometric fluorescence measurements of membrane potential. *Biochemistry* 28:4536–4539.
33. Briggman KL, Abarbanel HD, Kristan WB, Jr. (2005) Optical imaging of neuronal populations during decision-making. *Science* 307:896–901.
34. Salzberg BM, Grinvald A, Cohen LB, Davila HV, Ross WN (1977) Optical recording of neuronal activity in an invertebrate central nervous system: Simultaneous monitoring of several neurons. *J Neurophysiol* 40:1281–1291.
35. Ross WN, Arechiga H, Nicholls JG (1987) Optical recording of calcium and voltage transients following impulses in cell bodies and processes of identified leech neurons in culture. *J Neurosci* 7:3877–3887.
36. Taylor AL, Cottrell GW, Kleinfeld D, Kristan WB, Jr. (2003) Imaging reveals synaptic targets of a swim-terminating neuron in the leech CNS. *J Neurosci* 23:11402–11410.
37. Briggman KL, Kristan WB, Jr. (2006) Imaging dedicated and multifunctional neural circuits generating distinct behaviors. *J Neurosci* 26:10925–10933.
38. Baca SM, Marin-Burgin A, Wagenaar DA, Kristan WB, Jr. (2008) Widespread inhibition proportional to excitation controls the gain of a leech behavioral circuit. *Neuron* 57: 276–289.
39. Briggman KL, Kristan WB, Jr., Gonzalez JE, Kleinfeld D, Tsien RY (2010) Monitoring integrated activity of individual neurons using FRET-based voltage-sensitive dyes. *Membrane Potential Imaging in the Nervous System: Methods and Applications*, eds Canepari M, Zecevic D (Springer, New York), pp 61–70.
40. Ataka K, Pieribone VA (2002) A genetically targetable fluorescent probe of channel gating with rapid kinetics. *Biophys J* 82:509–516.
41. Perron A, et al. (2009) Second and third generation voltage-sensitive fluorescent proteins for monitoring membrane potential. *Front Mol Neurosci* 2:5.
42. Siegel MS, Isacoff EY (1997) A genetically encoded optical probe of membrane voltage. *Neuron* 19:735–741.
43. Kralj JM, Hochbaum DR, Douglass AD, Cohen AE (2011) Electrical spiking in *Escherichia coli* probed with a fluorescent voltage-indicating protein. *Science* 333:345–348.
44. Sjulson L, Miesenböck G (2007) Optical recording of action potentials and other discrete physiological events: A perspective from signal detection theory. *Physiology (Bethesda)* 22:47–55.
45. Fernández JM, Taylor RE, Bezanilla F (1983) Induced capacitance in the squid giant axon. Lipophilic ion displacement currents. *J Gen Physiol* 82:331–346.
46. Loew LM, Bonneville GW, Surow J (1978) Charge shift optical probes of membrane potential. Theory. *Biochemistry* 17:4065–4071.
47. Kuhn B, Fromherz P (2003) Anellated hemicyanine dyes in a neuron membrane: Molecular Stark effect and optical voltage recording. *J Phys Chem B* 107:7903–7913.
48. Kuhn B, Fromherz P, Denk W (2004) High sensitivity of Stark-shift voltage-sensing dyes by one- or two-photon excitation near the red spectral edge. *Biophys J* 87: 631–639.
49. Ueno T, et al. (2004) Rational principles for modulating fluorescence properties of fluorescein. *J Am Chem Soc* 126:14079–14085.

Supplementary Appendix for

Optically monitoring voltage in neurons by photoinduced electron transfer through molecular wires

Evan W. Miller,[1] John Y. Lin,[1] E. Paxon Frady,[2] Paul Steinbach,[3] William B. Kristan, Jr.,[2] Roger Y. Tsien[1,3,4]

[1]Departments of Pharmacology, [2]Neurosciences Graduate Group, [3]Howard Hughes Medical Institute, [4]Division of Biological Sciences, and [5]Department of Chemistry & Biochemistry, University of California San Diego, 9500 Gilman Drive, La Jolla, California, 92093-0647, USA.

Corresponding Author: Roger Y. Tsien, UCSD, 310 George Palade Laboratory, 9500 Gilman Drive, La Jolla, California, 92093-0647; rtsien@ucsd.edu; (858) 534-4891.

Methods

Imaging, electrophysiology, and cell culture.

HEK293 cells were cultured in DMEM (CellGrow) supplemented with 10% FBS, 1% penicillin/streptomycin (Invitrogen) and plated on glassbottom culture dishes (35 mm dish, 14 mm microwell with No. 0 coverglass) (MatTek Corporation). Hippocampal neurons were dissected from postnatal day 0 or 1 rat pups and plated on poly-D-lysine-coated glassbottom culture dishes. Neuronal recordings were made 14-28 days in culture.

Electrophysiological recordings of HEK293 cells and cultured neurons were performed with an Axopatch 200A or 200B amplifier (Molecular Devices) at room temperature. The signals were digitized with Digidata 1332A and recorded with pCLAMP 9 software (Molecular Devices) on a PC. Analysis of electrophysiological data was done with AxoGraph X (AxoGraphX), pCLAMP 9, and/or ClampFit (Molecular Devices). For most experiments the extracellular solution consisted of (in mM) 145 NaCl, 20 glucose, 10 HEPES, 3 KCl, 2 $CaCl_2$, 1 $MgCl_2$ (pH 7.35, 310 mOsm). The intracellular solution contained (in mM) 115 potassium gluconate, 10 BAPTA tetrapotassium salt, 10 HEPES, 5 NaCl, 10 KCl, 2 ATP disodium salt, 0.3 GTP trisodium salt (pH 7.25, 290 mOsm).

For studies to determine excitation sensitivity of dyes, illumination was provided by a Polychrom IV light source (T.I.L.L. Photonics GMBH) with a mechanical shutter (Uniblitz VS25). For all other studies, light was provided by an Xenon arc lamp powered by an Optiquip Power supply

(Optiquip) with a mechanical shutter controlled by a Lambda 10-2 controller (Sutter). Light from the Xenon arc lamp was filtered through a 480 nm filter (30 nm bandpass, Chroma), a 510 nm dichroic (Semrock), a 530 nm emission filter (50 nm bandpass, Semrock), and focused through a 40x/1.4 oil objective. For di-4-ANEPPS imaging, a 625 nm emission filter with a 50 nm bandpass was used. Bleaching studies used identical illumination conditions (480/30 nm excitation, 510 nm dichroic, 7 W/cm^2 output) and were corrected by normalizing for the extinction coefficient at the excitation wavelengths (465-495 nm).

Epifluorescence images were acquired with either a Cascade II 512, CoolSNAP cf2 or Evolve 128 (Photometrics) controlled with Slidebook software (Intelligent Imaging Innovations). Confocal images were acquired on a Zeiss LSM 5Live confocal microscope (Zeiss). For confocal imaging, a 40x/1.2 water objective was used, along with excitation provided at 488 nm by an argon laser. Emission was collected with a 505 nm longpass filter after passage through a 490 nm dichroic/beamsplitter.

To measure the speed of VF2.4.Cl response, the camera was replaced with a PMT (Hamamatsu). A diaphragm inserted into the light path allowed sampling of fluorescence from just the patch-clamped cell. A brief (10 ms) depolarization was delivered and both the optical and electrophysiological signals were recorded at a sampling rate of 50 kHz. 100 trials were averaged and the resulting rise and fall times were fit using Clampfit software (Molecular Devices).

Leech imaging and physiology.

Isolated midbody ganglia (Ganglia 8-16) were dissected from *Hirudo medicinalis* and the ventral side was desheathed using standard procedures. The voltage sensitive dye was combined with HEPES saline down to the desired concentration (100-300 nM), and 1.5 µL of a 20% (w/v) solution of Pluronic F-127 in DMSO. The dye was then continuously pumped over the ganglion to help with penetration into the cell membranes for 20-30 minutes. This follows similar procedure with the coumarin partner of the FRET voltage dye pair.[1]

Electrophysiological measurements were made with paired electrode recordings with resistances in the range of 20-40 MΩm. Electrode 1 acted as the recording electrode, which constantly monitored membrane potential, and electrode 2 acted as the current injecting electrode. Capacitance measurements were made by injecting 1 nA square wave of

hyperpolarizing current into the cell. The resulting decaying exponential approach of the membrane potential towards a hyperpolarized steady state was normalized to its minimum and maximum values and compared across the different conditions (**Fig. 2d**). The capacitance C was calculated with the formula C = tau * I / ΔV, where I = 1 nA and the hyperpolarization ΔV was 15-18 mV. Tau was measured two ways: 1) the time required for the normalized curve to reach (1-1/e); 2) the time constant of the best fit exponential or sum of exponentials. Neither measure changed the quality of the result showing that no capacitative load was added with the PeT-VSD, while significant load was added with the FRET dye. Spontaneous Retzius cell activity was measured with a single electrode.

Imaging was done with a Cascade 128+ EMCCD camera (Photometrics). The filter set was standard for FITC. The fluorescence illumination was from an LED that has its peak excitation wave-length in the excitation range for FITC.Image acquisition rates for the spontaneous imaging were made at 50Hz at 128x128 pixel resolution under a 20x, 0.5NA objective (Fig 5). The high-frequency imaging of the Retzius action potential (Fig S3b) was done at 722Hz (the maximum rate achievable for this camera with 1 ms exposure time), with 4x4 pixel binning (32x32 pixel resolution), under a 40x, 0.8NA objective. The binning and higher NA of the objective allowed for faster acquisition rates and for more light collection, bringing the light-levels high enough to be above the dark noise of the camera. Acquisition and analysis were run with custom-made software. The data is stored in Matlab-readable files.

Data Analysis

For voltage sensitivity measurements, regions of interest were drawn around clamped cells and the mean fluorescence measured in ImageJ or Slidebook. For HEK cells, background fluorescence was subtracted by measuring the fluorescence where no cells grew. For experiments in neurons, the background fluorescence was not subtracted. In all cases, ΔF/F was calculated by dividing the fluorescence signal by the average fluorescence for a baseline of 10-20 frames prior to stimulation.

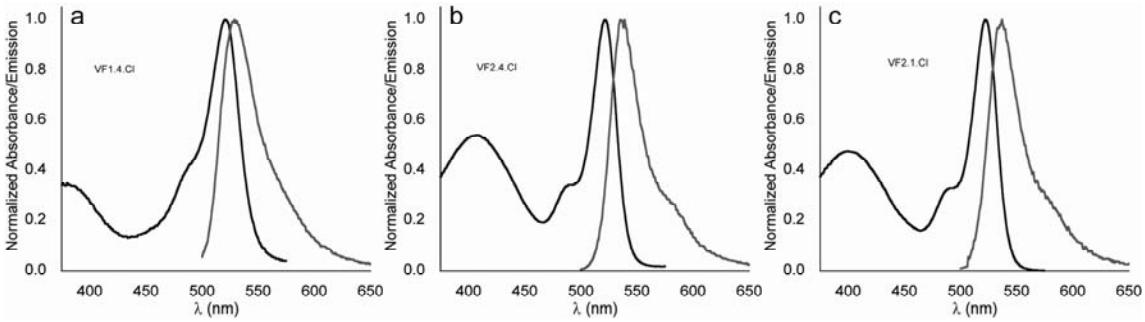

SI Figure 1: Normalized absorbance and emission spectra for VF dyes in 5 mM sodium phosphate, pH 9 with 0.1% Triton X-100. Black lines are absorbance spectra; grey lines are emission spectra. a) VF1.4.CI, b) VF2.4.CI, and c) VF2.1.CI.

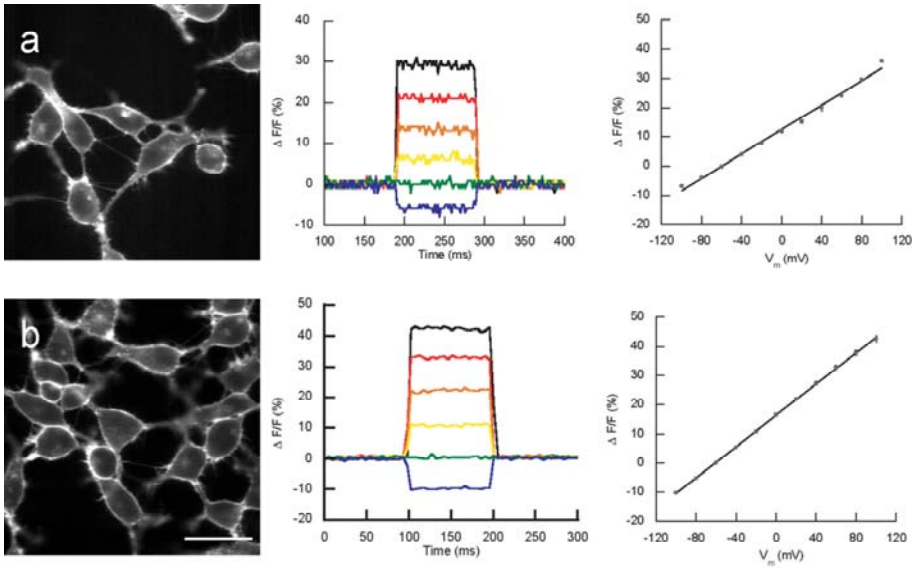

SI Figure 2: Characterization of VoltageFluor sensors in HEK cells. Confocal images of HEK 293 cells stained with a) 2 μM VF1.4.CI or b) 100 nM VF2.1.CI. (*middle*) Fractional changes in VF1.4.CI (*upper*) or VF2.1.CI (*upper*) fluorescence during a series of voltage steps to +100 or -100 from a holding potential of -60 mV (40 mV increments). (*right*) Fractional changes in VF1.4.CI (*upper*) or VF2.1.CI (*lower*) fluorescence plotted against membrane potential for voltage changes from a holding potential of -60 mV. Each data point represents 3-4 separate measurements. Error bars are S.E.M. Scale bar = 20 μm.

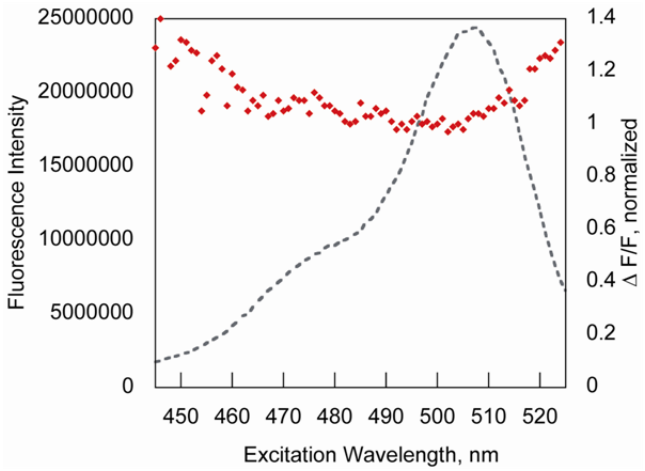

SI Figure 3 Wavelength sensitivity of CaGreen. Dotted grey spectrum shows an excitation scan of CaGreen in 100 mM Na MOPS with 1 mM EDTA. Red dots depict the normalized fluorescent response to the addition of excess (4 mM Ca^{2+}) vs. the excitation wavelength. The relatively invariant fluorescent response is characteristic of PeT-based fluorescent sensors.

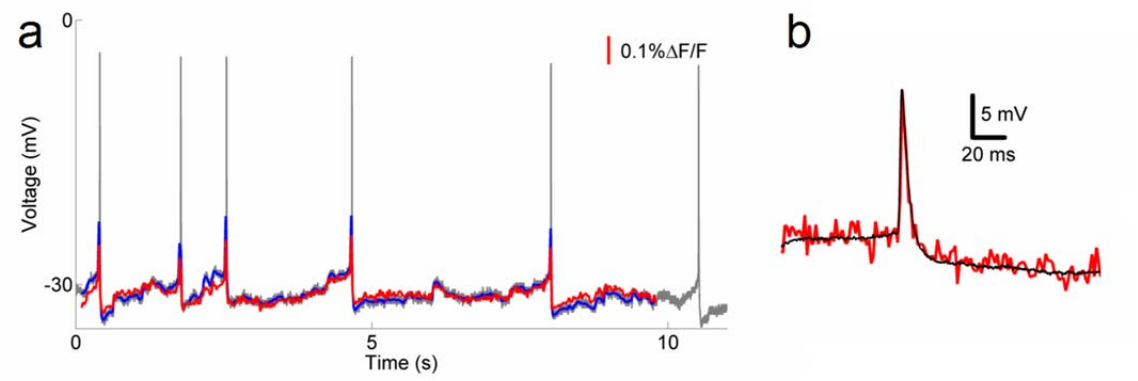

SI Figure 4:
Sampling action potentials at slow and fast rates. **a)** Same data as **shown in Figure 3c**. The red trace is a hi-pass filtered VF2.1.Cl optical signal sampled at 50 Hz. The electrophysiological trace has been faded to gray for clarity. The blue trace is the electrophysiological trace sampled at 50 Hz, which shows a similar variability in amplitudes of the action potentials due to the lower sampling rate. **b)** High-frequency sampling of VF2.1.Cl. The sampling rate of the optical data was increased to 722 Hz by binning pixels in the CCD camera. The optical trace (red) fully follows the Retzius cell action potential (black). However, increased electronic noise decreases the signal-to-noise ratio of the optical signal, making imaging at this rate suboptimal for accurate measurements of the slower, subthreshold signals.

Theoretical Considerations

To estimate the externally-detectable amount of charge transfer driven by light, we start by noting that each dye molecule of extinction coefficient ε (in units of $M^{-1}cm^{-1}$) has an optical

cross-section σ (in cm^2) of ε(1000 cm^3/L)(ln 10)/N_0, where N_0 is Avogadro's number. For reasonably monochromatic light of intensity *W* (in watts/cm^2) at wavelength λ, the photon flux *I* (in photons•$cm^{-2}s^{-1}$) is *W*λ/*hc*, where *h* and *c* are Planck's constant and the speed of light respectively. Each dye molecule is excited at a rate of *I*σ (units of s^{-1}), after which it has a probability *p* of undergoing photoinduced electron transfer (PeT), in which an electron of charge *q* (= 1.602 x 10^{-19} coulombs) travels a fraction η of the thickness of the insulating portion of the membrane. The mean charge displacement per unit time detectable outside the membrane is *I*σ*pq*η. Each charge pulse lasts for τ seconds before the electron returns to its original position by electron-hole recombination. At steady state in a population of dye molecules (at a surface density *S* in molecules/cm^2) asynchronously absorbing photons, the forward and backwards currents are both of magnitude *SI*σ*pq*η and cancel each other out. However, after a sudden change of membrane potential has changed *p* to *p*', the rate of forward charge displacement due to PeT will be *SI*σ*p'q*η, whereas for a time τ the rate of backward charge displacement due to charge recombination will still be *SI*σ*pq*η. Therefore the net charge displacement will be *SI*σ(Δ*p*)*q*ητ. Note that the charge movement is strictly dependent on illumination, unlike the voltage-driven movement of a lipid soluble ion or a gating charge on an ion channel.

A crude upper limit on the surface density *S* is 10^5 molecules/$(\mu m)^2$ = 10^{13} molecules/cm^2, corresponding to about 1 dye molecule per 10 phospholipid molecules in the outer leaflet. We know ε at 480 nm = 2.5 x $10^4 M^{-1}cm^{-1}$, from which σ = 9.55 x 10^{-17} cm^2. Our typical excitation intensity W at 480 nm is 0.7 W/cm^2, from which the photon flux *I* is 1.76 x 10^{18} photons/(cm^2s) and Iσ = 162 s^{-1}. If we assume *p* = 0.5, then Δ*p* would need to be 0.1 to explain a 20% change in fluorescence intensity for 100 mV depolarization. The distance from the aniline nitrogen to the highly hydrophilic sulfonate group, ~1.7 nm, is a reasonable upper limit for the distance that the electron could travel within the low-dielectric region of the membrane, whose overall thickness is ~3 nm^2, so an upper limit on η is 0.57. The greatest uncertainty is in τ, the lifetime of the PeT state before charge recombination back to the ground state. Rate constants for charge recombination in other donor-wire-acceptor examples[3,4] range from 10^6 to >10^9 s^{-1}, corresponding to τ = 1 μs to <1 ns. The shorter values of τ come from molecular wires similar in length to ours, whereas the higher τ values are from much longer wires. Nevertheless, if we take 1 μs as a conservative upper limit, the net charge displacement *SI*σ(Δ*p*)*q*ητ is 1.5 x 10^{-11} coul/cm^2. For comparison, when a typical biological membrane of 1 μF/cm^2 is depolarized by 100 mV, the ordinary capacitative charge is 10^{-7}coul/cm^2. Therefore the voltage sensor will add at most 0.015% to the capacitative load. The key reason this is so negligible is that each molecule spends only *I*στ (<<0.1%) of its time in the PeT state. If lipid-soluble ions could be

loaded at the same density *S*, and if their probability for residing on either surface were to change by $\Delta p = 0.1$, and if their η were 0.63 as measured for dipicrylamine in squid axon membranes[5], their charge displacement $S(\Delta p)q\eta$ would be 1.0×10^{-7} coul/cm^2, which would double the total capacitative load.

General Synthetic and Analytical Methods

$Pd(OAc)_2$ was from Strem Chemicals. All other chemicals were purchased from Sigma-Aldrich and used as received unless otherwise noted. 2',7'-dichloro-5-iodosulfofluorescein (**2**) was synthesized according to literature procedure.[6] Anhydrous solvents and reagents (THF, DMF, NEt_3) were obtained as SureSeal bottles from Sigma-Aldrich. Thin-layer chromatography and flash chromatography were performed using EMD pre-coated silica gel 60 F-254 plates and silica gel 60 (230-400 mesh). Alumina was activity 1, 70-230 mesh.

UV absorbance and fluorescence spectra were recorded on a Cary 3E (Varian) and Fluorolog 2 (Spex) fluorimeter, respectively. Analytical, semi-preparative, and preparative HPLCs were performed on Agilent HPLCs, with Luna C18(2) columns (Phenomenex) using water (solvent A) and acetonitrile (solvent B) with 0.05% TFA as an additive. Low resolution ESI mass spectrometry was performed on an Agilent LC/MSD Trap XCT coupled to an Agilent HPLC. High resolution mass spectra were acquired on a ThermoFisher Orbitrap XL hybrid mass spectrometer. ^{1}H NMR spectra were collected in $CDCl_3$ or d_6-DMSO (Cambridge Isotope Laboratories, Cambridge, MA) at 25 ºC on a 400 Varian Mercury Plus or Jeol ECA 500 spectrometer at the Department of Chemistry and Biochemistry NMR Facility at the University of California, San Diego. All chemical shifts are reported in the standard δ notation of parts per million using the peak of residual proton signals of $CDCl_3$ or d_6-DMSO as an internal reference.

Chemical Synthesis

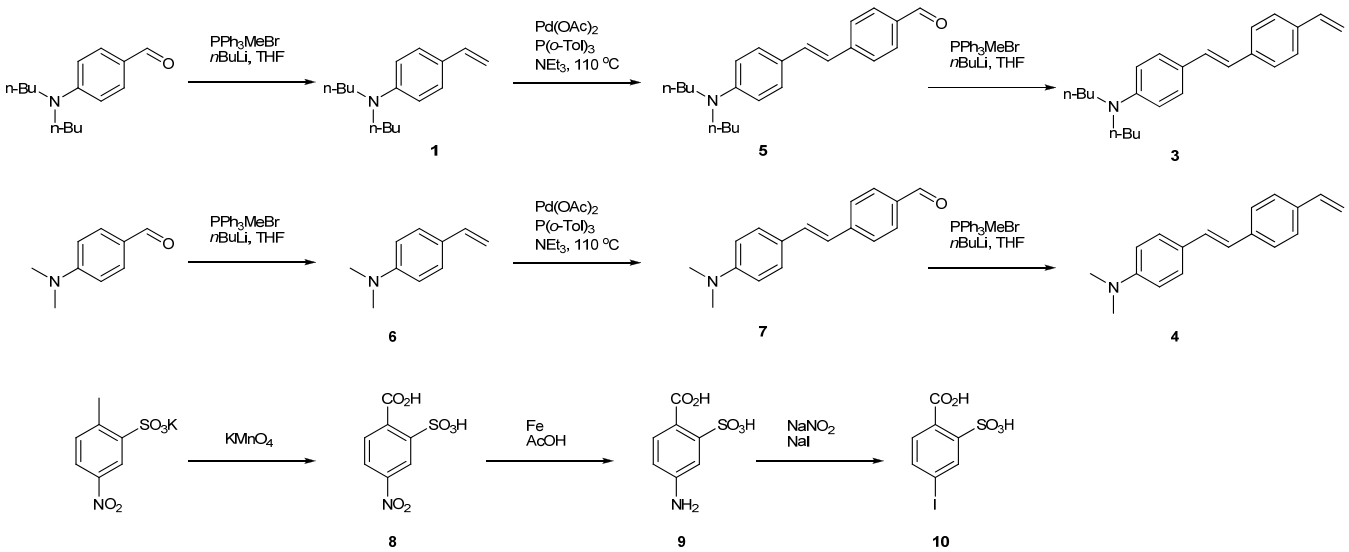

Synthesis of *N,N*-dibutyl-4-aminostyrene (**1**)

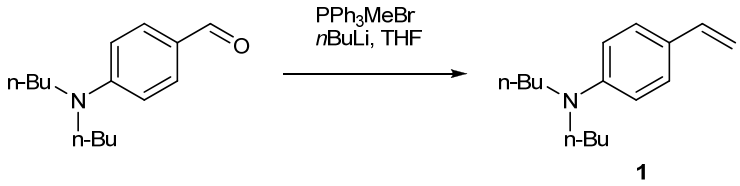

An oven-dried roundbottom flask was charged with methyltriphenylphosphonium bromide (1.4 g, 3.9 mmol, 1.8 equiv.) and 10 mL anhydrous THF and stirred under N_2. A 1.6 M solution of *n*-butyllithium in hexanes was added via syringe (2.2 mL, 3.5 mmol, 1.6 equiv.) at room temperature. After stirring for 15 min, 4-N,N-dimethylbenzaldehyde (508 mg, 2.2 mmol, 1.0 equiv.) was added. After stirring overnight, the reaction was poured into 100 mL of hexanes. The suspension was filtered through Celite and concentrated under reduced pressure. The residue was taken up in EtOAc and filtered through a thin pad (1-2 cm) of silica. Removal of solvents under reduced pressure provided 505 mg of a yellow oil (99%) which was judged to be pure by ^{1}H NMR. δ($CDCl_3$): 7.28 (2H, d, *J* = 8.6 Hz); 6.60 (3H, m); 5.50 (1H, d, *J* = 17.8 Hz); 4.98 (1H, d, *J* = 10.3 Hz); 3.27 (4H, m); 1.57 (4H, q, *J* = 7.4 Hz); 1.35 (4H, sextet, *J* = 7.4 Hz); 0.96 (6H, t, *J* = 7.4 Hz).

Synthesis of (E)-4-(4-(dibutylamino)styryl)benzaldehyde (**5**)

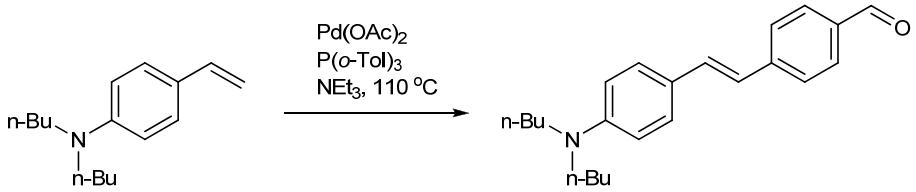

1 **5**

An oven-dried screw cap vial was equipped with a stir bar and charged with 4-bromobenzaldehyde (832 mg, 4.5 mmol, 1.0 equiv.), $Pd(OAc)_2$ (10 mg, 0.045 mmol, 0.01 equiv.), tri-*o*-tolylphosphine (27 mg, 0.09 mmol, 0.02 equiv.), and (**1**) (1.3 g, 5.6 mmol, 1.25 equiv.). The flask was evacuated and backfilled three times with N_2. Triethylamine (2.25 mL) was added, the vial sealed, and heated at 110°C. After stirring 20 hours, the reaction vessel was cooled to room temperature, dissolved in EtOAc and washed with saturated NaCl. The organic portions were dried over Na_2SO_4, filtered, and concentrated under reduced pressure. The orange residue was recrystalized from hexanes to give **5** as orange-yellow needles, 1.2 g (64%). ^{1}H NMR. δ($CDCl_3$): 9.94 (1H, s); 7.82 (2H, d, *J* = 8.0 Hz); 7.58 (2H, d, *J* = 8.6 Hz); 7.40 (2H, d, *J* = 9.2 Hz); 7.19 (1H, d, *J* = 16.6 Hz); 6.89 (1H, d, *J* = 16.0 Hz); 6.62 (2H, d, *J* = 8.6 Hz); 3.30 (4H, m); 1.58 (4H, m); 1.36 (4H, sextet, *J* = 7.4 Hz); 0.96 (6H, t, *J* = 7.4 Hz).

Synthesis of (E)-N,N-dibutyl-4-(4-vinylstyryl)aniline (**3**)

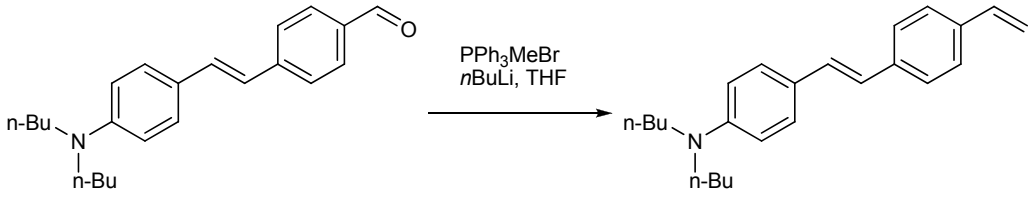

5 **3**

An oven-dried two-neck round bottom flask was cooled under N_2 and charged with methyltriphenylphosphonium bromide (2.1 g, 5.9 mmol, 1.8 equiv.) and anhydrous THF (15 mL). A 1.6 M solution of *n*-butyllithium in hexanes was added via syringe (3.3 mL, 5.3 mmol, 1.6 equiv.) and stirred for 15 minutes at ambient temperature. A solution of **5** (1.1g, 3.3 mmol, 1.0 equiv.) in THF (5 mL) was added with stirring. After stirring 12 hours, the reaction mixture was dissolved in CH_2Cl_2, filtered through a thin plug of alumina (1-2 cm), eluting with CH_2Cl_2. The organics were removed under reduced pressure to give a yellow solid which was triturated with EtOH. The resulting pale yellow solid was filtered and washed with EtOH to give (**3**), 958 mg (87%). ^{1}H NMR. δ ($CDCl_3$): 8.53 (2H, d, *J* = 8.5 Hz); 7.36 (4H, d, *J* = 7.0 Hz); 7.03 (1H, d, *J* = 16.6 Hz); 6.85 (1H, d, *J* = 16.6 Hz); 6.70 (1H, dd, J_1 = 17.0 Hz, J_2 = 10.8 Hz); 6.62 (2H, d, *J* =

8.5 Hz); 5.73 (1H, d, *J* = 17.6 Hz); 5.20 (1H, d, *J* = 11.5 Hz); 3.28 (4H, t, *J* = 7.5 Hz); 1.58 (4H, m); 1.36 (4H, sextet, *J* = 7.5 Hz); 0.96 (6H, t, *J* = 7.5 Hz).

Synthesis of *N*,*N*-dimethyl-4-vinylaniline (**6**)

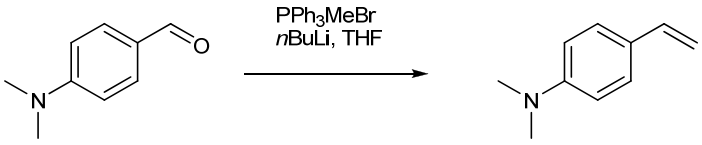

6

An oven-dried roundbottom flask was charged with methyltriphenylphosphonium bromide (4.3 g, 3.9 mmol, 1.8 equiv.) and 30 mL anhydrous THF and stirred under N_2. A 1.6 M solution of *n*-butyllithium in hexanes was added via syringe (6.7 mL, 10.7 mmol, 1.6 equiv.) at room temperature. After stirring for 15 min, 4-N,N-dimethylbenzaldehyde (1.0 g, 6.7 mmol, 1.0 equiv.) was added. After stirring overnight, the reaction was poured into 100 mL of hexanes. The suspension was filtered through Celite and concentrated under reduced pressure. The residue was taken up in EtOAc and filtered through a thin pad (1-2 cm) of alumina. Removal of solvents under reduced pressure provided 870 mg of **6** as a yellow oil (88%) which was judged to be pure by ^{1}H NMR. δ($CDCl_3$): 7.30 (2H, d, *J* = 8.5 Hz); 6.68 (2H, d, *J* = 9.0 Hz); 6.63 (1H, dd, J_1 = 17.6 Hz, J_2 = 11.0 Hz); 5.53 (1H, d, *J* = 17.6 Hz); 5.01 (1H, d, *J* = 10.5 Hz); 2.95 (6H, s).

Synthesis of (E)-4-(4-(dimethylamino)styryl)benzaldehyde (**7**)

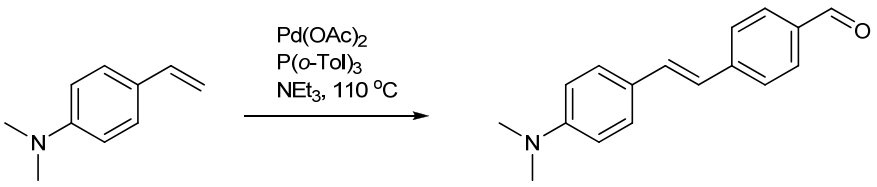

6 **7**

An oven-dried screw cap vial was equipped with a stir bar and charged with 4-bromobenzaldehyde (775 mg, 4.2 mmol, 1.0 equiv.), $Pd(OAc)_2$ (9.4 mg, 0.042 mmol, 0.01 equiv.), tri-*o*-tolylphosphine (25.5 mg, 0.084 mmol, 0.02 equiv.), and N,N-dimethyl-4-vinylaniline (770 mg, 5.2 mmol, 1.25 equiv.). The flask was evacuated and backfilled three times with N_2. Triethylamine (2.5 mL) was added, the vial sealed, and heated at 110°C. After stirring 20 hours, the reaction vessel was cooled to room temperature, dissolved in CH_2Cl_2 and washed with saturated NH_4Cl, followed by saturated NaCl. The organic portions were dried over Na_2SO_4, filtered, and concentrated under reduced pressure. The orange residue was taken up in a minimal amount of CH_2Cl_2 and crystalization was induced by addition of excess hexanes.

Trituration with hexanes provided 970 mg of **7** (92%). ^{1}H NMR. δ($CDCl_3$): 9.95 (1H, s); 7.82 (2H, d, *J* = 8.0 Hz); 7.59 (2H, d, *J* = 8.6 Hz); 7.44 (2H, d, *J* = 9.2 Hz); 7.20 (1H, d, *J* = 16.0 Hz); 6.93 (1H, d, *J* = 16.0 Hz); 6.71 (2H, d, *J* = 8.6 Hz); 3.0 (6H, s).

Synthesis of (E)-N,N-dimethyl-4-(4-vinylstyryl)aniline (**4**)

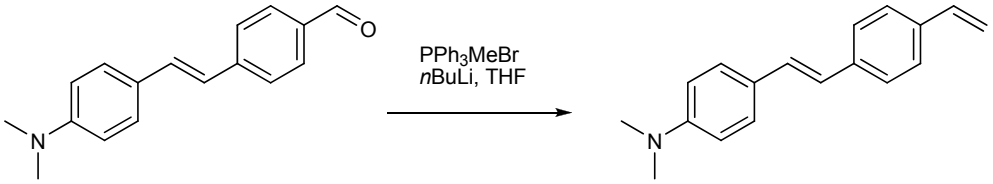

7 **4**

An oven-dried two-neck round bottom flask was cooled under N_2 and charged with methyltriphenylphosphonium bromide (950 mg, 6.8 mmol, 1.8 equiv.) and anhydrous THF (15 mL). A 1.6 M solution of *n*-butyllithium in hexanes was added via syringe (3.8 mL, 6.1 mmol, 1.6 equiv.) and stirred for 15 minutes at ambient temperature. A solution of **7** (950 mg, 3.8 mmol, 1.0 equiv.) in THF (5 mL) was added with stirring. After stirring 12 hours, the reaction mixture was dissolved in CH_2Cl_2, filtered through a thin plug of alumina (1-2 cm), eluting with CH_2Cl_2. The organics were removed under reduced pressure to give a yellow solid which was triturated with EtOH. The resulting pale yellow solid was filtered and washed with EtOH to give (**4**), 621 mg (66%). ^{1}H NMR. δ ($CDCl_3$): 7.40 (6H, m); 7.04 (1H, d, *J* = 16.6 Hz); 6.89 (1H, d, *J* = 16.6 Hz); 6.70 (3H, m); 5.73 (1H, d, *J* = 17.6 Hz); 5.21 (1H, d, *J* = 11.0 Hz); 2.98 (6H, s).

Synthesis of 4-nitro-2-sulfobenzoic acid (**8**)

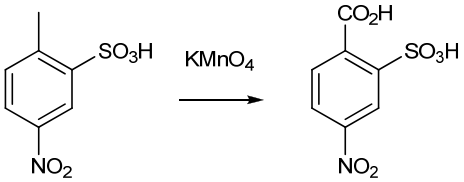

8

To a slurry of $KMnO_4$ (15 g, 96 mmol, 4 equiv.) in 120 mL water was added 30 mL of a solution of 4-nitrotoluene-2-sulfonic acid dihydrate (6.0 g, 24 mmol, 1.0 equiv.). The reaction vessel was fitted with a reflux condenser and the reaction heated at reflux for 4 hours. The reaction was cooled on ice and filtered to give a tan solution. The solid precipitate was washed with 200 mL of water, and the filtrate was then concentrated under reduced pressure to give about 100 mL. This was cooled on ice and acidified with concentrated HCl until the pH was less than 1. The mixture was heated to dissolve the white precipitate which formed, and cooled slowly to form

white crystals. After storing overnight at 4 °C, the off-white crystals were filtered, washed with 1-2 mL of cold water, and dried on a Büchner funnel to give 4.0 g (67%) of **8** as an off-white/peach solid that was judged to be 90% pure by ^{1}H NMR. ^{1}H NMR: δ (d_6-DMSO): 8.48 (1H, d, *J* = 2.5 Hz); 8.24 (1H, dd, J_1 = 8.3 Hz, J_2 = 2.5 Hz); 7.70 (1H, d, *J* = 8.0 Hz). ESI-MS, $[M-H]^-$ = 246.

Synthesis of 4-amino-2-sulfobenzoic acid, (**9**)

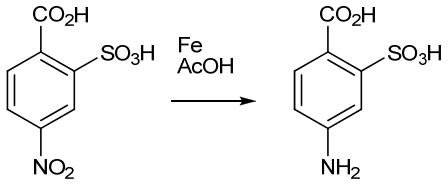

8 **9**

4-nitro-2-sulfobenzoic acid (4.0 g, 16.2 mmol, 1.0 equiv.) was dissolved in 12.5 mL of water and stirred in a 300 mL round bottom flask fitted with a reflux condenser. The reaction was heated to boiling, at which point all of **8** dissolved. 2.5 mL glacial acetic acid was added, followed by 6.35 g of Fe (113 mmol, 7.0 equiv.) in ~0.5 g portions every 15 minutes to avoid excessive bubbling. Upon completion of addition, the reaction was 6maintained at reflux for an additional 60 minutes. The reaction was cooled to room temperature, transferred to an Erlenmeyer flask, heated to boiling, and filtered while hot to remove unreacted iron. The solid was washed with several portions of boiling water (about 100 mL total). The pale green filtrate was again heated to boiling and filtered through a thin pad of Celite to get a pale orange solution. This was concentrated under reduced pressure, cooled on ice, and acidified with concentrated HCl until the pH was less than 1 and a yellow color/precipitate persisted. This was recrystalized from boiling water (about 100 mL total) and stored overnight at 4 °C. The yellow solid was filtered to get 1.32 g of **9**. The mother liquor was placed back in the cold room for two more days. A second crop of crystals was isolated, 230 mg. The crops were pooled to give 1.55 g of **9**, which was pure by ^{1}H NMR. ^{1}H NMR: δ (d_6-DMSO): 7.65 (1H, d, *J* = 8.5 Hz); 7.16 (1H, d, *J* = 2.0 Hz); 6.62 (1H, d, *J* = 8.0 Hz). ESI-MS, $[M-H]^-$ = 216

Synthesis of 4-iodo-2-sulfobenzoic acid (**10**)

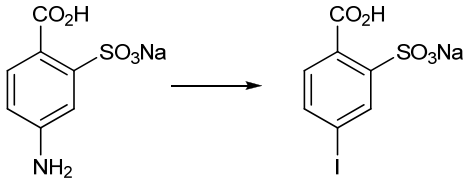

9 **10**

The hydrochloride salt of 4-amino-2-sulfobenzoic acid (**9**) was suspended in 10 mL H_2O. Na_2CO_3 was added (500 mg) and the reaction stirred until the solution was homogenous and the pH was about 8. After cooling on ice, $NaNO_2$ (355 mg, 5.2 mmol, 1.12 equiv.) dissolved in 1 mL H_2O was added. This solution was cooled on ice. With stirring, HCl (1 mL concentrated HCl diluted in 5 g crushed ice) was added and stirring continued on ice for 30 minutes. A solution of NaI (828 mg, 5.5 mmol, 1.2 equiv.) in 1 mL H_2O (cooled on ice) was added dropwise. The reaction went dark and produced gas. Stirring was maintained for 2 hours on ice, then 1 hour at room temperature and finally at 50 °C overnight. The following morning, 3 drops of conc. HCl were added and the reaction was concentrated on the rotovap to give a red/orange solid. This was recrystalized from boiling H_2O (<20 mL). Filtered the fluffy orange crystals to get 925 mg of **10**. The mother liquor was concentrated to dryness and recrystalized again to get an additional 315 mg (76% yield, total). ^{1}H NMR: δ (d_6-DMSO): 8.10 (1H, d, J = 1.5 Hz); 7.86 (1H, dd, J_1 = 8.0 Hz, J_2 = 1.5 Hz); 7.42 (1H, d, J = 8.0 Hz). ESI-MS, $[M+H]^+$ = 329, $[M-H]^-$ = 327.

Synthesis of 5-(4-(4-(dibutylamino)styryl)styryl)-2-(2,7-dichloro-6-hydroxy-3-oxo-3H-xanthen-9-yl)benzenesulfonic acid, Voltage Fluor 2.4.Cl (**VF2.4.Cl**)

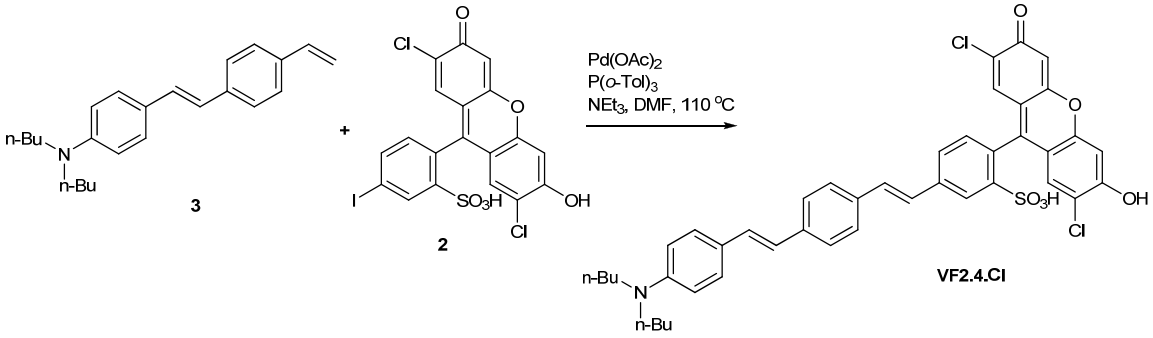

An oven-dried, N_2-cooled reaction tube was charged with 10 mg (17.8 µmol, 1.0 equiv.) of **2**, 6.6 mg (19.6 µmol, 1.1 equiv.) of styrene **3**, 1 mg (4.5 µmol, 0.25 equiv.) $Pd(OAc)_2$, 3 mg (9.0 µmol, 0.5 equiv.) of tri-*o*-tolylphosphine and a stirbar. The tube was fitted with a septum and evacuated and backfilled with N_2 three times. 100 µL of DMF and 50 µL of NEt_3 (0.36 mmol, 20 equiv.) were added via syringe, the septum replaced, and the reaction stirred at 110° C overnight. After stirring 12 hours, the reaction was cooled to room temperature, concentrated under reduced pressure, and taken up in CH_2Cl_2 and dilute aqueous KOH. After extracting 3x with CH_2Cl_2, the combined organic layers were extracted twice with dilute aqueous KOH. The pooled aqueous fractions were cooled on ice, and then acidified with cold concentrated HCl. A fine red solid precipitated out and this was filtered on a Büchner funnel, washed with Et_2O, and dried to give 14.4 mg of a brick red solid. This crude product was taken up in 200 µL of DMSO.

200 µL of MeCN was added to induce precipitation, and the resulting orange/brown solid was filtered on a Büchner funnel to give 9.6 mg (70%) of VF1. Samples for analytical measurements were further purified by preparative HPLC. ^{1}H NMR (500 MHz, d_6-DMSO) δ: 8.14 (1H, d, J = 1.2 Hz); 7.76 (1H, dd, J_1 = 8.0 Hz, J_2 = 1.7 Hz); 7.64 (2.5H, d, J = 8.0 Hz); 7.53 (2.5 Hz, d, J = 8.0 Hz); 7.41 (2.5H, d, J = 16.6 Hz); 7.36 (2.5H, d, J = 16.6 Hz); 7.22 (1H, d, J = 8.0 Hz); 7.15 (1H, m); 6.95 (3H, s); 6.72 (1H, bs); 6.61 (1H, bs); 3.26 (4H, t, J = 6.9 Hz); 1.47(4H, m); 1.29 (4H, sextet, J = 7.4 Hz); 0.89 (6H, t, J = 7.4 Hz). HR-ESI, calculated for $C_{43}H_{39}Cl_2NO_6S$, 767.1875, found [M^+] = 767.1888.

Synthesis of 5-(4-(4-(dimethyllamino)styryl)styryl)-2-(2,7-dichloro-6-hydroxy-3-oxo-3H-xanthen-9-yl)benzenesulfonic acid, Voltage Fluor 2.1.Cl (**VF2.1.Cl**)

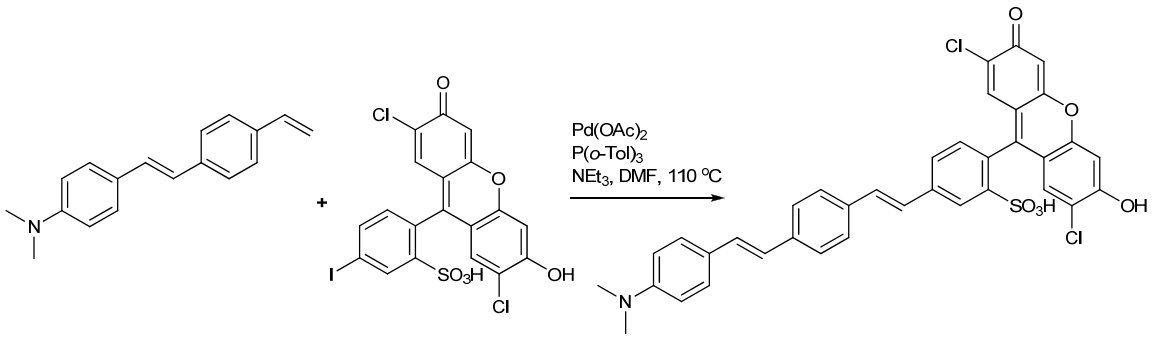

4 2 VF2.1.Cl

An oven-dried, N_2-cooled reaction tube was charged with 8 mg (14 µmol, 1.0 equiv.) of **4**, 3.9 mg (16 µmol, 1.1 equiv.) of (E)-N,N-dimethyl-4-(4-vinylstyryl)aniline, 1 mg (4.5 µmol, 0.32 equiv.) $Pd(OAc)_2$, 3 mg (9.0 µmol, 0.7 equiv.) of tri-*o*-tolylphosphine and a stirbar. The tube was fitted with a septum and evacuated and backfilled with N_2 three times. 500 µL of DMF and 50 µL of NEt_3 (0.36 mmol, 25 equiv.) were added via syringe, the septum replaced, and the reaction stirred at 110° C overnight. After stirring 12 hours, the reaction was cooled to room temperature, concentrated under reduced pressure, and concentrated down several times from CH_2Cl_2/hexanes to get a reddish brown solid. Took up in 1N NaOH to get a murky solution which was cooled on ice and acidified with concentrated HCl. The ensuing precipitate was filtered and dried on a Büchner funnel and washed with water and diethyl ether. This residue was dissolved in 400 µL 1:1 DMSO:MeCN and purified by preparative HPLC to give 5.6 mg of a tan/orange solid (51% yield).

^{1}H NMR (500 MHz, d_6-DMSO) δ: 8.14 (1H, d, J = 1.7 Hz); 8.10 (1H, s);7.76 (1H, dd, J_1 = 8.0 Hz, J_2 = 1.2 Hz); 7.64 (2H, d, J = 8.0 Hz); 7.55 (2H, d, J = 8.6 Hz); 7.45 (2H, d, J = 8.6 Hz); 7.42 (1H, d, J = 16.6 Hz); 7.36 (1H, d, J = 16.6 Hz); 7.22 (1H, d, J = 8.0 Hz); 7.18 (1H, d, J = 16.6

Hz); 7.00 (1H, d, *J* = 16.6 Hz); 6.95,(2H, s); 6.76 (1H, bs); 6.72 (2H, bs); 2.93 (6H, s). HR-ESI, calculated for $C_{37}H_{27}Cl_2NO_6S$, 683.0936, found [M^+] = 683.0933.

Synthesis of (E)-5-(4-(dibutylamino)styryl)-2-(2,7-dichloro-6-hydroxy-3-oxo-3H-xanthen-9-yl)benzenesulfonic acid, Voltage Fluor 1.4.Cl (**VF1.4.Cl**)

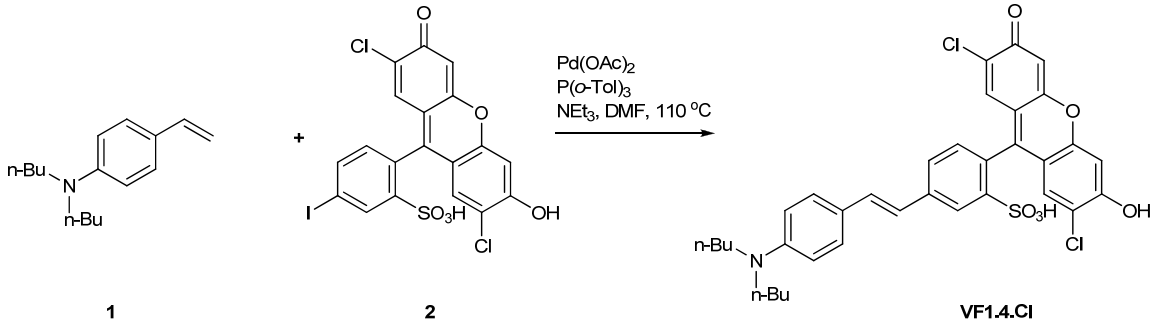

An oven-dried, N_2-cooled reaction tube was charged with 10 mg (17.8 µmol, 1.0 equiv.) of **2**, 4.5 mg (19.6 µmol, 1.1 equiv.) of *N,N*-dibutyl-4-vinylaniline **1**, 1 mg (4.5 µmol, 0.25 equiv.) $Pd(OAc)_2$, 3 mg (9.0 µmol, 0.5 equiv.) of tri-*o*-tolylphosphine and a stirbar. The tube was fitted with a septum and evacuated and backfilled with N_2 three times. 100 µL of DMF and 100 µL of NEt_3 (0.72 mmol, 40 equiv.) were added via syringe, the septum replaced, and the reaction stirred at 110° C overnight. After stirring 12 hours, the reaction was cooled to room temperature, diluted a 1N solution of NaOH and washed 3x with CH_2Cl_2. The aqueous layer was concentrated to near dryness, acidified with 10% HCl, cooled on ice, and filtered. The crude residue was taken up in 1:1 DMSO:MeCN, filtered through a 0.22 µm nylon spin filter, and purified by preparative HPLC.

^{1}H NMR (500 MHz, d_6-DMSO) δ: 8.10 (1H, s); 8.04 (1H, d, *J* = 1.7 Hz); 7.65 (1H, d, *J* = 1.7 Hz); 7.64 (1H, d, *J* = 1.7 Hz); 7.44 (2H, d, *J* = 8.6 Hz); 7.22 (1H, d, *J* = 16.0 Hz); 7.14 (1H, d, *J* = 8.0 Hz); 7.05 (1H, d, *J* = 16.0 Hz); 6.95 (2H, bs); 6.63 (2H, d, *J* = 8.6 Hz); 1.49 (4H, quintet, *J* = 7.4 Hz); 1.30 (4H, sextet, *J* = 7.4 Hz); 0.90 (6H, t, *J* = 7.4 Hz). HR-ESI, calculated for $C_{35}H_{33}Cl_2NO_6S$, 665.1406, found [M^+] = 665.1382.

References

1. Briggman, K.L., Abarbanel, H.D. & Kristan, W.B., Jr. Optical imaging of neuronal populations during decision-making. *Science* **307**, 896-901 (2005).
2. Andersen, O.S. & Koeppe, R.E., 2nd. Bilayer thickness and membrane protein function: an energetic perspective. *Ann. Rev. Biophys.Biomol.Struct.* **36**, 107-30 (2007).
3. Davis, W.B., Svec, W.A., Ratner, M.A. & Wasielewski, M.R. Molecular-wire behaviour in p-phenylenevinylene oligomers. *Nature* **396**, 60-63 (1998).

4. de la Torre, G., Giacalone, F., Segura, J.L., Martin, N. & Guldi, D.M. Electronic communication through pi-conjugated wires in covalently linked porphyrin/C-60 ensembles. *Chem. Eur. J.* **11**, 1267-1280 (2005).
5. Fernandez, J.M., Taylor, R.E. & Bezanilla, F. Induced capacitance in the squid giant axon. *J. Gen. Physiol.* **82**, 331-346 (1983).
6. Jiao, G.S., Han, J.W. & Burgess, K. Syntheses of regioisomerically pure 5-or 6-halogenated fluoreseeins. *J. Org. Chem.* **68**, 8264-8267 (2003).